Eur. Phys. J. A **13**, 501–515 (2002)
DOI 10.1140/epja/iepja1308

THE EUROPEAN PHYSICAL JOURNAL A

Propagation of mesons in asymmetric nuclear matter in a density-dependent coupling model

R. Aguirre[a] and A.L. De Paoli

Department of Physics, La Plata National University, C.C. 67 (1900) La Plata, Argentina

Received: 16 October 2001 / Revised version: 10 January 2002
Communicated by V. Vento

Abstract. We study the propagation of the light mesons σ, ω, ρ, and $a_0(980)$ in dense hadronic matter in an extended derivative scalar coupling model. Within the scheme proposed it is possible to unambiguously define effective density-dependent couplings at the Lagrangian level. We first apply the model to study asymmetric nuclear matter with fixed isospin asymmetry, and then we pay particular attention to hypermatter in β-equilibrium. The equation of state and the potential contribution to the symmetry coefficient arising from the mean-field approximation are investigated.

PACS. 21.30.Fe Forces in hadronic systems and effective interactions – 21.65.+f Nuclear matter – 12.40.Yx Hadron mass models and calculations – 26.60.+c Nuclear matter aspects of neutron stars

1 Introduction

In recent years the medium dependence of the meson-baryon couplings has been object of speculation [1–9]. This subject has been advertised by the successes of the so-called quantum-hadrodynamics theory (QHD) [10], in the relativistic description of nuclear phenomena.

The assumption of variable couplings in the mean-field approximation (MFA) is founded on different grounds. It can be interpreted as the trace of the quark structure of hadrons [7–9], or it can be viewed as a way to match effective Lagrangians and free-space nucleon-nucleon interactions [1–6]. In any case assigning a variable behavior to the couplings seems to be an appropriate method to interpolate from one dynamical regime to another, using effective hadron field models. A similar meaning has been given to the in-medium meson masses, which have been related to the transition to the chiral regime [11]. The so-called Brown-Rho scaling law qualitatively describes the behaviour of the hadronic masses in the proximity of the transition point. According to the scaling law, all hadronic masses decrease approximately at the same rate as the system approaches to the chiral phase transition (with exception of the pseudo-scalar meson masses).

On the other hand, in certain purely hadronic models [12,13] the non-polynomial meson-nucleon interaction gives rise to effective, density-dependent coupling in the MFA [14–16].

At this point it is worthwhile to mention that the use of effective chiral models in hadron physics became mandatory in the last years in regard of the attempts to relate hadronic phenomenology with the fundamental theory of strong interactions. This requirement is specially relevant for the study of the few-nucleons problem or of hadronic matter at very low baryonic density. In these cases the detailed structure of the interaction is very significative. This fact is in apparent contradiction with the successes obtained by using models that do not exhibit an explicit chiral symmetry, as for instance the Walecka model. In this case even the use of pionic degrees of freedom is avoided. However, in ref. [17] it was shown the essential coherence of certain chiral models and the Walecka one, in the MFA, for the medium- and high-density regime. Thus the Walecka model can be regarded as the remaining interaction when certain degrees of freedom are integrated out. In this sense, there exists a large amount of work, see for example [18], supporting the interpretation of the σ-meson interaction as a correlated interchange of pions. Also, the inclusion of non-linear σ-meson couplings within the frame of these models seems to be necessary in order to describe appropriately the main properties of nuclear matter and finite nuclei. An example of this feature is the Derivative Scalar Coupling model (DSCM) [13], where a non-polynomial σ-meson coupling with baryons is proposed. According to the present discussion, a treatment of all the mesons on the same foot of equality is desirable if one wants to generalize the DSCM in order to interprete it as a high-density limit of chiral models like, for example, the Nambu–Jona-Lasinio model [19].

In this work we want to move in this direction, taking the DSCM as our starting point. Furthermore a modified version of this model is proposed to explore the high-

[a] e-mail: aguirre@venus.fisica.unlp.edu.ar

density behavior of nuclear matter with hyperons in conditions that may exist in the interior of neutron stars. In our model the charge symmetry is preserved and it provides effective couplings for all the mesonic channels considered. The medium dependence comes through the mean value of the scalar σ-meson, evaluated at finite density and temperature. More general interactions could include nonlinear vertices in terms of all the mesons considered, but we restrict here to the simplest case. This choice is similar to the approach of [3], where the functional dependence of the couplings includes only the product $\bar{\Psi}\gamma_\mu\Psi$, but not the scalar $\bar{\Psi}\Psi$ or more involved nucleon field combinations. As stressed in this reference, the density variation of the couplings must be written as a Lorentz invariant functional of the fields, to obtain the correct Euler-Lagrange equations. Otherwise the so-called "rearrangement" contribution is absent and the thermodynamical consistency is lost.

We use the model proposed here to investigate asymmetric nuclear matter at finite temperature, therefore we explicitly include the isovector mesons ρ and $a_0(980)$.

The equation of state of asymmetric matter is an important input in astrophysical studies such as the cooling rate of neutron stars or the supernova collapse mechanism. It is well known that the proton concentration is determinant in the cooling of neutron stars [20,21], and this concentration is mainly determined by the isospin-dependent contribution to the equation of state.

As an interesting case of asymmetric matter we consider hadronic matter in β-equilibrium. For this purpose we generalize the DSCM model to include the octet of baryons n, Λ, Σ, and Ξ.

We want to stress that our results are expected to be valid at sufficiently high density, therefore we have selected applications within the scope of astrophysical interest. Extrapolations to heavy-ion collision scenarios could not be necessarily valid.

We have evaluated the meson propagators in the relativistic random phase approximation (RRPA), including particle-antiparticle contributions, and we have extracted from them the in-medium effective meson masses. The scalar-meson masses cannot be unambiguously determined, instead we use a regularizing parameter to explore their potential regimes of variation.

We organize this paper presenting the model in sect. 2, in sect. 3 we discuss the bulk properties of symmetric nuclear matter at zero temperature, meanwhile the asymmetric nuclear matter equation of state is treated in sect. 4. The properties of β-stable matter are considered in sect. 5, and the Feynman graphs contributing to the RRPA, the evaluation of the propagators and the behavior of mesons in the hadronic environment are presented in sect. 6. We conclude with the discussion and summary in sect. 7.

2 The modified DSCM

In this section we present a relativistic model of hadronic fields inspired on the DSCM proposed by Zimanyi and Moszkowski [13]. The DSCM has been used to study nuclear many-body effects in several applications [22], to investigate neutron star properties [23], extended to include nucleon resonances [24] and hyperons [25], related to an effective quark description of hadronic properties [26], and generalized with a tensor coupling [27] in order to improve the spin-orbit splitting.

The DSCM has two important features which distinguish it from the QHD-I model of ref. [10]. In first place it is non-renormalizable *ab initio* and there is no immediate way to introduce vacuum corrections to the MFA to the ground state, although the main properties of nuclear matter are successfully described. In second place a residual interaction can be extracted beyond the lowest order solution, whose strength decreases monotonically as a function of the baryonic density [15,16]. This fact ensures the ground state predominance at high density as assumed in QHD [10].

Since we are interested here in the description of asymmetric matter, besides the fields Ψ^a for the nucleons, we include the isoscalar scalar (σ) and isoscalar vector (ω_μ) mesonic fields, and those corresponding to the ρ isovector vector (ρ^A_μ) and the $a_0(980)$ isovector scalar (δ^A) mesons. We use Greek, Latin lower case and Latin upper case indexes to denote Lorentz, baryon isospin and meson isospin components, respectively.

In its simplest version the DSCM [13] has a Yukawa type N-ω coupling and a N-σ non-polynomic term. We modify the vertices allowing for two different mesons (one of them the scalar σ) to locally interact with a baryon:

$$\begin{aligned}\mathcal{L}_{\rm DSC} = \bar{\Psi}\left[i\ \partial\!\!\!/ - \frac{M - g_d\,\tau\cdot\delta + g_w\ \omega\!\!\!/ + g_r\tau\cdot\ \rho\!\!\!//2}{1+g_s\sigma/M}\right]\Psi \\ +\frac{1}{2}(\partial^\mu\sigma\partial_\mu\sigma - m_s^2\sigma^2) + \frac{1}{2}(\partial^\mu\delta\partial_\mu\delta - m_d^2\delta^2) \\ -\frac{1}{4}F^{\mu\nu}F_{\mu\nu} + \frac{1}{2}m_w^2\omega^2 - \frac{1}{4}\mathbf{R}^{\mu\nu}\mathbf{R}_{\mu\nu} + \frac{1}{2}m_r^2\rho^2, \quad (1)\end{aligned}$$

where $\Psi(x)$ is the isospin multiplet nucleon field, M is the averaged nucleon mass and g_s, g_d, g_v, and g_r are adimensional coupling constants. As usual in QHD the ground state for homogeneous infinite matter is approximated by considering mesonic fields as classical quantities and assimilating them to effective nucleon properties. Thus we can separate the c-number contributions:

$$\sigma(x) = \bar{\sigma} + s(x), \quad (2)$$

$$\delta^A(x) = \bar{\delta}\ \delta^{3A} + d^A(x), \quad (3)$$

$$\omega_\mu(x) = \bar{\omega}\ \delta_{\mu 0} + w_\mu(x), \quad (4)$$

$$\rho^A_\mu(x) = \bar{\rho}\ \delta_{\mu 0}\delta^{3A} + r^A_\mu(x), \quad (5)$$

where $\bar{\sigma}$, $\bar{\delta}$, $\bar{\omega}$, and $\bar{\rho}$ are classical mean-field values and s, d^A, w_μ, and r^A_μ are quantum fluctuations which are not included in the ground state. Expressions for the c-number contribution to meson fields can be obtained by taking statistical averaged Euler-Lagrange equations, and requiring

self-consistency. In this way we obtain

$$m_s^2\bar{\sigma} = g_s\frac{\langle\bar{\Psi}(M - g_d\tau_3\bar{\delta} + g_w\gamma_0\bar{\omega} + \frac{1}{2}g_r\tau_3\gamma_0\bar{\rho})\Psi\rangle}{MN^2}, \quad (6)$$

$$m_d^2\bar{\delta} = g_d\frac{\langle\bar{\Psi}\tau_3\Psi\rangle}{N}, \quad (7)$$

$$m_w^2\bar{\omega} = g_w\frac{\langle\Psi^\dagger\Psi\rangle}{N}, \quad (8)$$

$$m_r^2\bar{\rho} = g_r\frac{\langle\Psi^\dagger(\tau_3/2)\Psi\rangle}{N}, \quad (9)$$

where we have used $N = 1 + g_s\bar{\sigma}/M$. The expectation values must be evaluated with the ground-state solution for the nucleon field, which depends on $\bar{\sigma}$ and $\bar{\delta}$ through the effective nucleon mass

$$M_i^* = \frac{M - g_d I_i\bar{\delta}}{N}, \quad (10)$$

with $I_i = 1, -1$ for protons and neutrons, respectively. The nucleon dispersion relation is also modified according to $(p_0 - g_w\bar{\omega} - g_r I_i\bar{\rho}/2)^2 - p^2 = {M_i^*}^2$.

In eqs. (8) and (9) the terms between angular brackets represent the conserved baryon density and the isospin density, respectively.

A residual nucleon-meson interaction arises beyond the lowest order approximation [15] by inserting eqs. (2)-(5) in the interaction term:

$$\frac{M + \sum_i \Gamma_i\phi_i}{1 + g_s\sigma/M} = \frac{M + \sum_i \Gamma_i(\bar{\phi}_i + \delta\phi_i)}{N(1 + g_s s/N)}.$$

In the expression above the symbol ϕ_i represents any one of the mesonic fields δ, ω, and ρ, which by virtue of eqs. (3)-(5) splits into the classical mean value $\bar{\phi}_i$, and the quantum fluctuation $\delta\phi_i$. Γ_i stands for the bare meson-nucleon vertices: $\Gamma_i = -g_d\tau, g_w\gamma, g_r\tau\gamma/2$, corresponding to the a_0-, ω-, and ρ-meson, respectively. The right-hand side of this equation is non-polynomic and cannot be used to directly apply a diagrammatic expansion. Restricting to the physical regime for which quantum fluctuations are negligible compared to mean values, enables us to approximate:

$$\frac{M + \sum_i \Gamma_i\phi_i}{1 + g_s\sigma/M} \simeq M^* + \gamma_0\ \delta\varepsilon + \mathcal{L}_{\rm res}, \quad (11)$$

with

$$\delta\varepsilon = \sum_{\omega,\rho}\Gamma_i^*\bar{\phi}_i, \quad (12)$$

$$\mathcal{L}_{\rm res} = -g_s^* s + \sum_i \Gamma_i^*\left[\delta\phi_i - \frac{g_s}{NM}(\bar{\phi}_i + \delta\phi_i)s\right]. \quad (13)$$

We have introduced the medium-dependent vertices Γ_i^*, which are obtained from the bare ones by replacing the coupling constants g_d, g_w, and g_r by effective couplings. The last ones are given by the relation $g_d/g_d^* = g_w/g_w^* = g_r/g_r^* = N$. Also we have used $g_s/g_s^* = N^2$.

The expansion proposed in eq. (11) respects the organizational principle of nuclear effective field theories [28].

In this approximation, the residual interaction of eq. (13) arises besides the nucleon effective mass (10) and the contribution to the nucleon single-particle energy (12). The interaction term $\mathcal{L}_{\rm res}$ comprises a one-meson–nucleon vertex, together with a two-meson exchange term. In all cases the vertex functions are medium dependent, $g_s^*\left(1 + \sum_i \Gamma_i\bar{\phi}_i/M\right), \Gamma_d^*, \Gamma_w^*$, and Γ_r^* for the one-meson case and $g_s^*\Gamma_i/M$ for the two-meson instance.

This linearized version can be used to study the quantum corrections beyond the mean-field approximation.

Variable couplings are an expected feature of hadronic models, whenever the quark substructure becomes relevant [7–9]. Furthermore, density-dependent couplings have been proposed as a key assumption in order to match relativistic nucleon potentials adjusted to scattering data, with hadronic field models [1–6]. This approach was initiated as a way to avoid involved Brueckner-Hartree-Fock calculations for finite systems, using one-boson exchange potentials. Thus, the main purpose is to take advantage of the relative simplicity of the Hartree approach of the QHD models. The link between both schemes is established by requiring the equality of the nucleon self-energy in symmetric nuclear matter as evaluated in both formulations, and allowing QHD coupling constants to be density dependent.

In our treatment the effective couplings are unambiguously extracted from the Lagrangian, once the MFA has been introduced. Thus in this scheme one has a well-defined and invariant way to describe the medium influence on the couplings. Furthermore, the internal consistency of the approach is guaranteed.

Up to this point, we have restricted the discussion only to protons and neutrons, however the introduction of hyperons is straightforward. A sum over different baryonic species must be considered in the Lagrangian density and the vertices must be modified in order to take into account the isospin degeneracy of each one. Also, additional couplings between the mesons and every hyperon isomultiplet must be introduced. A more detailed discussion will be given in sect. 5.

The energy density E for infinite homogeneous hadronic matter, can be evaluated in the MFA by taking the statistical average of the energy momentum tensor: $E = \langle T^{00}\rangle$. The thermodynamical pressure P under the same conditions is obtained by averaging the trace of the spatial-spatial component of this tensor: $P = \langle{\rm Tr}\, T^{ij}\rangle/3$. We include the corresponding equations for the sake of completeness:

$$\begin{aligned} E = &\sum_{i=p,n}\frac{1}{(2\pi)^3}\int_0^\infty {\rm d}^3k E_{k\,i}\left[n_{\rm F}(E_{k\,i}) + n_{\rm F}(-E_{k\,i})\right] \\ &+\frac{1}{2}(m_s^2\bar{\sigma}^2 + m_d^2\bar{\delta}^2 - m_w^2\bar{\omega}^2 - m_r^2\bar{\rho}^2) \\ &+g_w^*\bar{\omega}\, n + \frac{1}{2}g_r^*\bar{\rho}\,(n_p - n_n), \end{aligned} \quad (14)$$

$$P = \sum_{i=p,n} \frac{1}{3(2\pi)^3} \int_0^\infty \mathrm{d}^3k \frac{k^2}{E_{k\,i}} \left[n_\mathrm{F}(E_{k\,i}) + n_\mathrm{F}(-E_{k\,i})\right] - \frac{1}{2}(m_s^2\bar{\sigma}^2 + m_d^2\bar{\delta}^2 - m_w^2\bar{\omega}^2 - m_r^2\bar{\rho}^2), \quad (15)$$

with $E_{k\,i} = \sqrt{M_i^{*2} + k^2}$, M_i^* is given by eq. (10), and

$$n_\mathrm{F}(z_i) = \frac{\Theta(z_i)}{1 + e^{\beta(x_i - \mu_i)}} + \frac{\Theta(-z_i)}{1 + e^{\beta(x_i + \mu_i)}},$$

is the nucleon statistical occupation number, $x_i = z_i + g_w\bar{\omega} + I_i g_r\bar{\rho}/2$ is the particle energy, μ_i is the chemical potential, and $\beta = 1/k_\mathrm{B}T$. The chemical potential is related to the number density of the i-type particle through:

$$n_i = \frac{1}{(2\pi)^3} \int_0^\infty \mathrm{d}^3k \left[n_\mathrm{F}(E_{k\,i}) - n_\mathrm{F}(-E_{k\,i})\right], \quad (16)$$

and finally $n = n_p + n_n$ is the total particle number density.

To evaluate eqs. (14) and (15), one must fix the particle number densities n_p, n_n and then simultaneously solve eqs. (6)-(10), together with eq. (16).

Another interesting quantity is the nuclear symmetry energy E_s defined as

$$E_\mathrm{s} = \frac{1}{2} \left.\frac{\partial^2 E}{\partial \chi^2}\right|_{\chi=0},$$

where $\chi = (n_n - n_p)/n$. This energy contains a purely kinetic term T, and a contribution V_s coming from the isovector mesons only. The explicit expression for E_s at zero temperature, including the a_0-meson contribution has been already derived, see for example [29]:

$$E_\mathrm{s} = T + V_\mathrm{s}, \quad (17)$$

$$T = \frac{1}{12} \sum_{i=p,n} \frac{p_{\mathrm{F}_i}^2}{E_{\mathrm{F}_i}}, \quad (18)$$

$$V_\mathrm{s} = g_r^{*2} \frac{n_0}{8m_r^2} - g_d^{*2} \frac{n_0 \sum_i \left(\frac{M_i^*}{E_{\mathrm{F}_i}}\right)^2}{4(m_d^2 + g_d^{*2}A)}, \quad (19)$$

where p_{F_i} is the Fermi momentum for the i-type particle, $E_{\mathrm{F}_i} = \sqrt{p_{\mathrm{F}_i}^2 + M_i^{*2}}$, and

$$A = \sum_{i=p,n} \frac{3}{\pi^2 E_{\mathrm{F}_i}} \left[M_i^{*2} p_{\mathrm{F}_i} + \frac{p_{\mathrm{F}_i}^3}{3} - M_i^{*2} E_{\mathrm{F}_i} \ln\left(\frac{p_{\mathrm{F}_i} + E_{\mathrm{F}_i}}{M_i^*}\right)\right].$$

3 Bulk properties of symmetric nuclear matter at T = 0

In the previous section we have presented the model, which contains several free parameters. The masses of the a_0-, ω- and ρ-meson are taken at their physical values

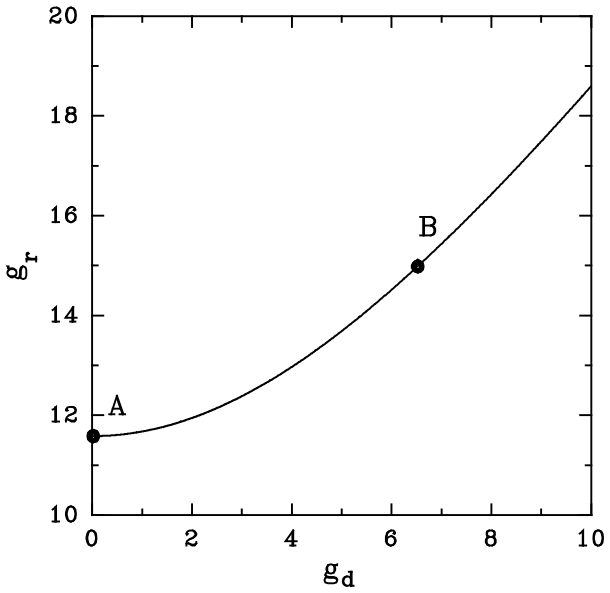

Fig. 1. The relationship between the couplings g_r and g_d, constrained to reproduce the symmetry energy $E_\mathrm{s} = 32$ MeV at zero temperature and at the saturation density n_0. The pair of couplings A and B used in our calculations are marked with circles.

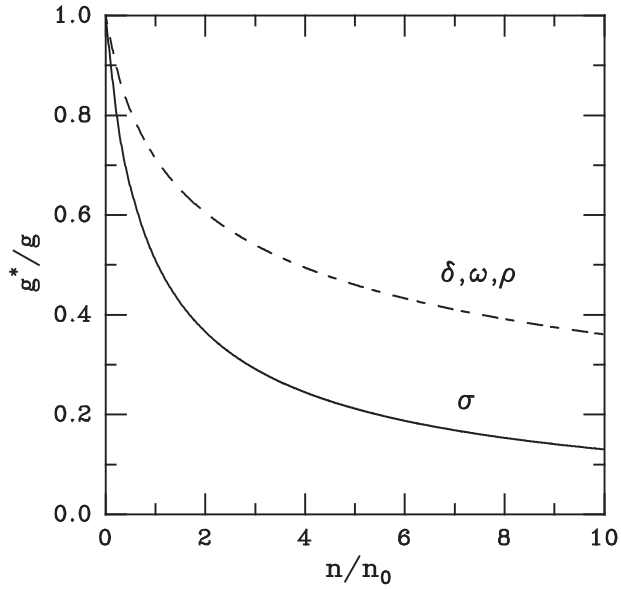

Fig. 2. The effective couplings relative to their vacuum values in symmetric nuclear matter at $T = 0$, in terms of the baryon density. The solid line corresponds to the σ channel, and the dashed line to the δ, ω, and ρ cases.

$m_d = 984$ MeV, $m_w = 783$ MeV, and $m_r = 770$ MeV, respectively. We adopt the accepted value for the σ-meson mass $m_s = 550$ MeV. There remains to determine the four coupling constants. We adjust them to reproduce the main bulk properties of symmetric nuclear matter: the saturation density $n_0 = 0.15\,\mathrm{fm}^{-3}$, the binding energy $\varepsilon_\mathrm{B} = -15$ MeV, and the symmetry energy $E_\mathrm{s} = 32$ MeV at zero temperature and at normal density. Another

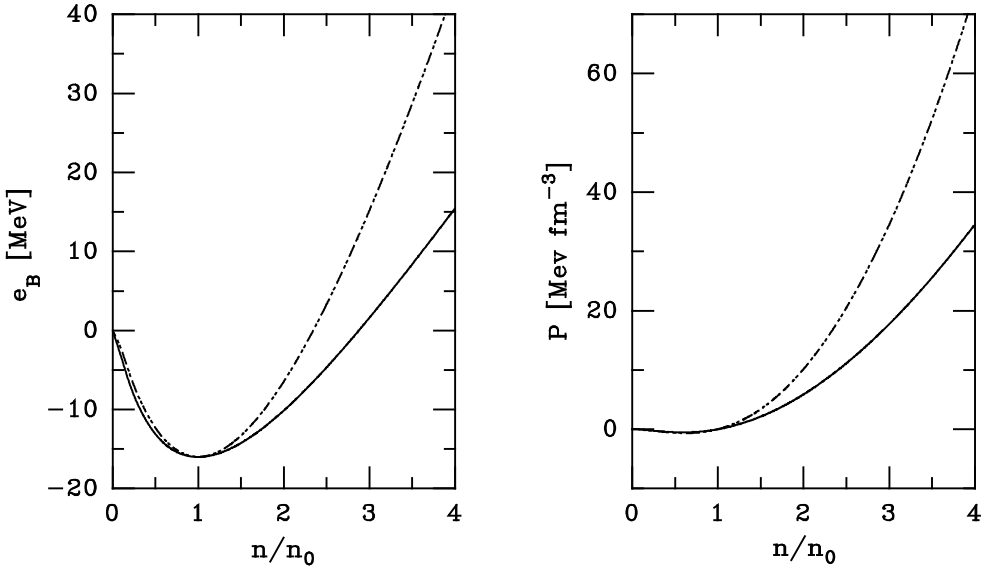

Fig. 3. The binding energy (left) and the pressure (right) as functions of the baryon number density at $T = 0$, in the MFA. Solid and dashed lines correspond to our results and the standard DSCM calculations, respectively.

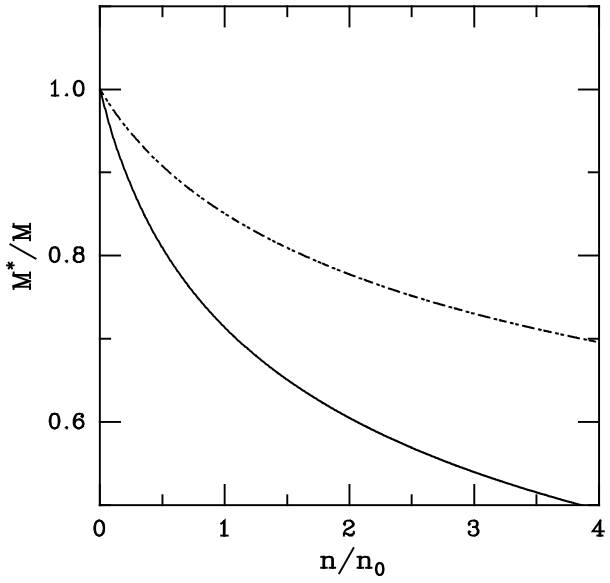

Fig. 4. The effective nucleon mass at zero temperature in symmetric nuclear matter. The line convention is the same as in fig. 3.

quantity of physical interest is the isothermal compressibility κ_T, however the DSCM provides very good values for κ_T without imposing any further condition. Therefore we have three physical conditions to fix the four coupling constants. Two of them, g_s and g_w are univocally determined as $g_s = 12.379$, $g_w = 14.624$, whereas g_r and g_d are functionally dependent through eqs. (17)-(19) evaluated at $n = n_0$. For our calculations we have selected two sets of couplings (g_r, g_d), denoted by A and B: set A $= (11.583, 0)$ and set B $= (15, 6.538)$, which are shown in fig. 1.

As previously mentioned, a feature of the model proposed is the presence of effective couplings. The behaviour of these couplings relative to their vacuum values is the same for the δ, ω, and ρ fields, and different for the scalar σ, as discussed in sect. 2. As can be seen in fig. 2, the channel corresponding to the last case is much more suppressed in dense matter. This figure corresponds to symmetric nuclear matter, but it must be noted that the behavior of the effective couplings depends on the composition of the hadronic medium, *i.e.* they must depend on the asymmetry coefficient χ.

We compare these results with the density-dependent hadron field theory (DDHFT) outcomes [3–6]. For this purpose we use the interpolating algebraic function given in [5]. Differences are appreciable at medium and high densities. The couplings for σ, ω, and ρ are monotonous decreasing in both formalisms. A dropping of 20% for the isoscalar mesons, and of 42% for the ρ-meson is detected in the DDHFT at $n/n_0 = 2$. Our results provide for the same conditions a stronger decay of 60% for the σ coupling and of 40% in the remaining cases.

With the sets of parameters A and B we have evaluated some properties of symmetric nuclear matter at zero temperature. In fig. 3 we compare our results for the binding energy and the pressure as functions of the baryon number density, with those corresponding to the standard DSCM. It can be seen that there are not appreciable differences below $n = 1.5\, n_0$, from here on both $\varepsilon_{\rm B}$ and P grow more slowly in our calculations. The isothermal compressibility is a measure of the stiffness of the pressure, we get at the saturation density $\kappa_T = 155$ MeV, against $\kappa_T = 220$ MeV for the DSCM. The lower slope of the binding energy in our results is essentially due to the weakening of the repulsion at higher densities induced by the normalization factor N. On the other hand, the relative difference between the mean values $\bar{\sigma}$ and $\bar{\omega}$ increases with n in our model, meanwhile in the standard DSCM it approaches to zero.

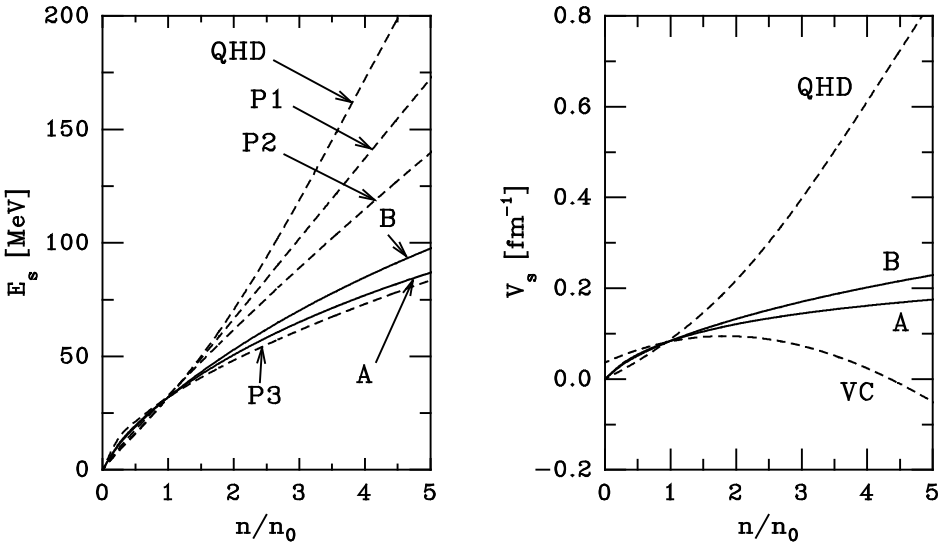

Fig. 5. The full symmetry energy (left panel) and the interaction contribution $V_{\rm s}$ (right panel), in terms of the baryon number density. In both cases solid lines correspond to results with coupling sets A and B. Dashed lines are used in the left panel for the QHD model (with δ contribution), and the parameterizations P1, P2 and P3 as explained in the text. On the right panel dashed lines correspond to the QHD model and to the parameterization given in ref. [30] for variational calculations (VC).

This gives rise to the relative lessening of the pressure at high densities in our results.

The medium effects on the effective nucleon mass can be seen in fig. 4, where a comparison with the DSCM result is made. In both cases M^* is positive definite and monotonous decreasing, but the rate of falling at densities $0 < n < 2\,n_0$ is more pronounced in our case because of the higher value of g_s needed to reproduce the normal properties of nuclear matter. At higher baryonic densities M^* stabilizes, due to the dynamical screening of the effective coupling.

As the next step we investigate the density dependence of the symmetry energy $E_{\rm s}$. It has been profusely studied in the past, using non-relativistic potentials as well as relativistic formulations [29–35]. Recently $E_{\rm s}$ has received attention by its applications to the study of the structure of nuclei with a large neutron excess, produced in the radioactive ion beam facilities. It is also a relevant subject in the evolution of neutron stars, determining the composition of the ground state and the cooling mechanism [20], or the phase transition to quark matter [30]. Furthermore, it has been proposed that the ratio of neutrons to protons in the pre-equilibrium stage of collisions between neutron-rich nuclei could distinguish the asymmetric contribution of the nuclear equation of state [31].

Different theoretical predictions for $E_{\rm s}$ produce rather dissimilar density dependences. In the left part of fig. 5 we compare our results for the symmetry energy coefficient, with and without the contribution of the a_0-meson, with other commonly used descriptions. We include the result from the QHD model of ref. [29] including the nucleon-a_0-meson coupling, and other three cases labeled P1, P2, and P3. The latter correspond to the phenomenological parameterizations [21]:

$$E_{\rm s} = \frac{3}{5}\left(2^{2/3}-1\right) e_{\rm F}\left[u^{2/3} - F(u)] + E_{\rm s0}F(u)\right],$$

where $u = n/n_0$, $e_{\rm F}$ is the non-relativistic Fermi energy at the saturation density, and the function $F(u)$ takes the forms $F_1(u) = 2u^2/(1+u)$, $F_2(u) = u$, and $F_3(u) = \sqrt{u}$ for the curves denoted as P1, P2 and P3, respectively. All the curves are almost coincident for densities $n < 1.5\,n_0$, but their mutual differences become significative for densities above that limit. The exception corresponds to the cases A and P3, which differ from each other only by negligible amounts in all the range of shown densities. From eq. (19) it can be seen that the contributions to $V_{\rm s}$ of the isovector δ and ρ-mesons are opposite in sign. However choosing $g_d \neq 0$ brings on an enhanced behaviour of $E_{\rm s}$, because the value of g_r required to adjust $E_{\rm s} = 32$ MeV at $n = n_0$ is bigger than g_d (see fig. 1). It must be noted that the rate of growth of the cases A, B, and P3 decreases with density, whereas it remains approximately constant for the curves P1, P2 and slowly increases for the QHD case.

The effect of polynomial self-interactions of the σ field in QHD models has been studied in [36]. Both, the inclusion of exchange terms and of the δ coupling in Hartree approximation enhance the density dependence of $E_{\rm s}$, and therefore diverge from curves A and B in the left part of fig. 5.

The behavior of $E_{\rm s}$ depends on the method of evaluation and the model of interaction used, the latter defines the $V_{\rm s}$ term. On the right part of fig. 5 we display the interaction contributions for $E_{\rm s}$ obtained with the sets A and B, and we compare them with $V_{\rm s}$ extracted from the QHD model of [29] and with the parameterization given by [30] for the variational calculations (VC) made in [37]. It can be seen that our results are intermediate between

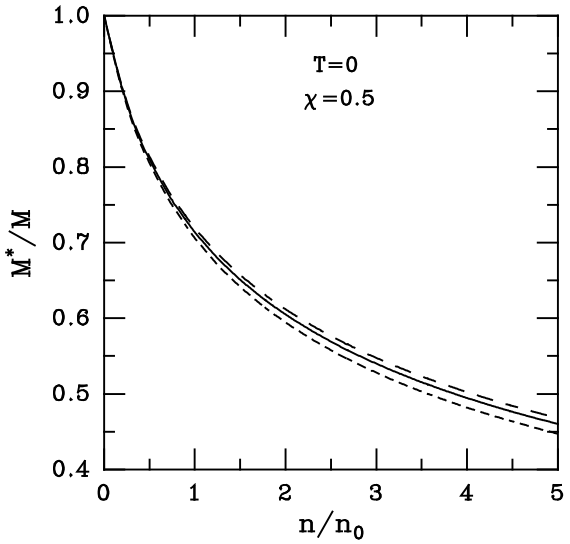

Fig. 6. The effective masses of proton and neutron as functions of the relative baryon number density for asymmetric nuclear matter at zero temperature. The solid (dashed) line corresponds to results with the coupling set A (B).

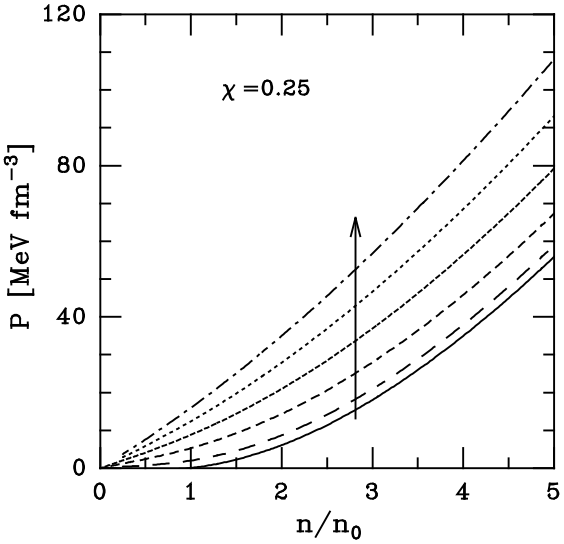

Fig. 7. The pressure P in terms of the nucleon number density at $\chi = 0.25$. The different curves correspond to temperatures $T = 0, 20, 40, 60, 80$, and 100 MeV. The arrow indicates the sense of growing temperatures. The results shown are obtained with the set A.

QHD and the VC results. A characteristic behaviour of the VC is that V_s becomes negative for densities greater than certain typical value, causing the disappearance of protons in neutron stars at high densities.

Curves QHD and B allow us to discern the effect of the medium-dependent couplings on the symmetry potential V_s. There are two sources of disagreement between both curves; in first place the density dependence of the effective nucleon mass of the model of ref. [29] are below the results of the modified ZM model. In second place, the couplings g_r and g_d are held fixed in the QHD calculations, whereas they decrease with density in the other case. Both effects induce coherently a faster increase of the QHD curve. A gross numerical estimate of their influence on the deviation shown for V_s at $n = 4n_0$ assigns about 70% to the medium-dependent couplings and 30% to the differences for the variation of the nucleon masses. From the behavior of the symmetry terms shown in fig. 5, we expect that the fraction of protons in star matter should be lower in our results as compared, for instance, with the QHD model prediction, although this fraction remains non-vanishing for all densities in our case. The inclusion of the δ coupling (curve B) slightly increases the presence of protons.

4 The equation of state of asymmetric nuclear matter

We study here the properties of nuclear matter at finite temperature by taking the asymmetry coefficient χ as a free parameter. In the next section the isospin asymmetry will be determined by the conditions of electric charge neutrality and matter stability against electroweak decay.

In first place we inspect the density dependence of the nucleon effective mass for fixed χ. In fig. 6 we compare results with and without δ coupling at $T = 0$ and $\chi = 0.5$. For $g_d = 0$ (set A) proton and neutron masses are degenerate, and for $g_d \neq 0$ (set B) the neutron (proton) mass is lowered (enhanced) due to medium effects. The splitting is heightened as the density increases.

Temperature effects are small in the range $0 < T < 100$ MeV, and more noticeable at high densities. For example, when the coupling set A is chosen, an increment of about 5 MeV in the nucleon effective mass is observed at $n = 5n_0$ as the temperature is raised from $T = 0$ to $T = 100$ MeV, at a given χ. Of the same magnitude but opposite in sign is the effect of increasing the asymmetry from $\chi = 0$ to $\chi = 1$ at a fixed temperature. When the coupling set B is used, it is found that the in-medium mass splitting $\Delta M^* = M_p^* - M_n^*$ decreases when the temperature is raised at fixed χ. On the other hand, ΔM^* is enhanced when the asymmetry is isothermally increased. Numerical values of this mass splitting depend on the set of couplings used, and we estimate the magnitude of both temperature and asymmetry effects calculating ΔM^* with the set B at $n = 5\,n_0$. In this case the splitting reduces about 5 MeV in neutron matter when the temperature covers the range $0 < T < 100$ MeV, but an increment of approximately 50 MeV is found in ΔM^* if χ is varied between $\chi = 0$ and $\chi = 1$ at fixed temperature.

The thermodynamical pressure P has been evaluated using eq. (15), for several temperatures $0 < T < 100$ MeV, and several asymmetries $0 < \chi < 1$. The increase of the temperature produces an enhancement of the pressure. This effect is strengthened by raising the asymmetry. The quantitative behavior of the pressure can be seen in figs. 7 and 8. In the first one we plot the pressure as a function of the number density at fixed asymmetry $\chi = 0.25$ and for several temperatures. For $T \geq 20$ MeV it is a monotonous increasing function of the density, whereas for $T = 0$ it

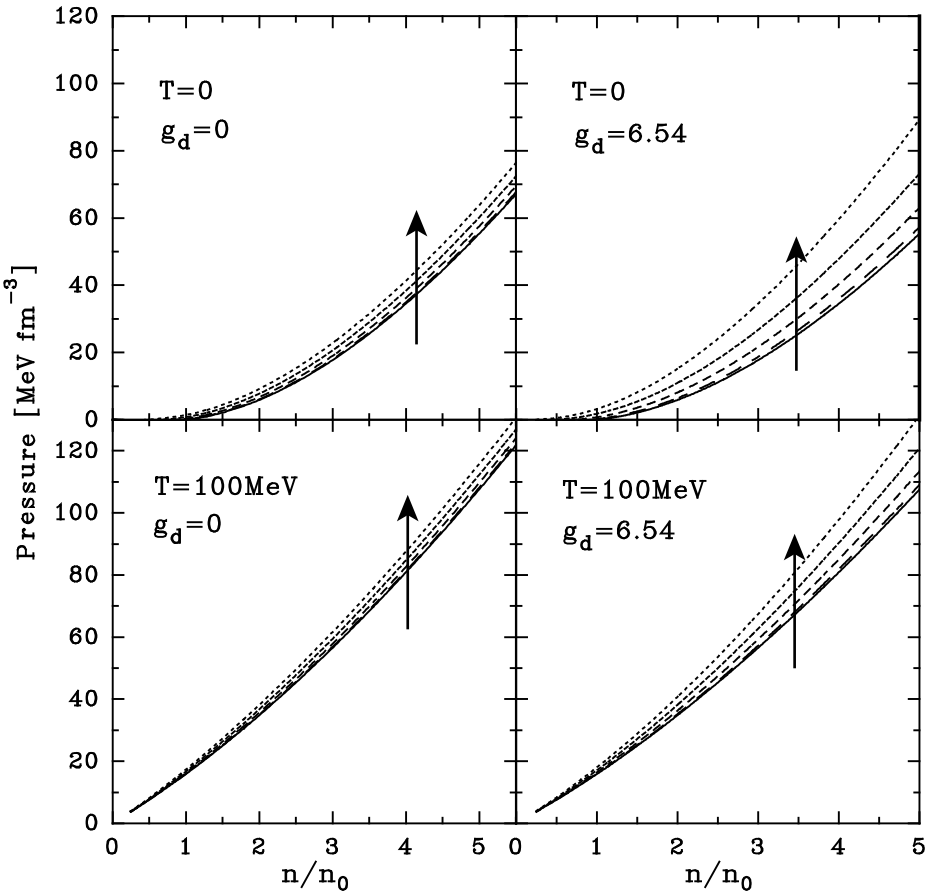

Fig. 8. The pressure as a function of the nucleon number density. Different types of lines correspond to the asymmetry coefficients $\chi = 0, 0.25, 0.50, 0.75$, and 1.0, respectively. The arrows indicate the direction of increasing χ. The top (bottom) panel represents calculations for $T = 0$ ($T = 100$ MeV), and the left (right) side is devoted to results using the coupling set A (B).

exhibits a region of instability for densities below n_0. This instability gives rise to a liquid-gas phase transition [10]. The results in fig. 7 correspond to the set A. By using the set B qualitatively similar results are obtained.

The relevance of the asymmetry in our calculations can be observed in fig. 8. The higher the values of the asymmetry the stiffer the pressure raises, this effect is emphasized when the coupling g_d is non-zero. The liquid-gas instability remains for low T and n, disappearing for χ close to 1.

5 Hadronic matter in β-equilibrium.

The conditions in the interior of certain stellar objects like protoneutron stars, require additional degrees of freedom to be included in the Lagrangian density of sect. 2. Due to the large densities reached in such systems, several physical phenomena could take place. The appearance of mesons and baryons with strangeness, pion and/or kaon condensation, the chiral symmetry restoration, and the phase transition to a quark-gluon plasma are some of the expected processes. They must be taken into account, in order to properly describe the high density behavior of the equation of state. In this section we complete the model proposed by including the hyperons Λ, Σ, and Ξ, but we do not treat explicitly the chiral symmetry and quark degrees of freedom. Therefore our results should be valid until fluctuations preceding any phase transition become relevant. However we present here calculations in the range $0 < n/n_0 < 10$ for the sake of comparison.

As anticipated in sect. 2, the modifications in the Lagrangian density are straightforward since we retain the form of the interaction for all the baryons. A sum over the full octet N, Λ, Σ, and Ξ must be considered in eq. (1), and new couplings g_s, g_d, g_w, and g_r are introduced for the hyperons. Furthermore, the vertex between the ρ-meson and the baryon B must be modified by including an appropriate coefficient: $I_{\rm B3} = 1/2$ for proton and Ξ^0, $I_{\rm B3} = -1/2$ for neutron and Ξ^-, $I_{\rm B3} = 1$ for Σ^+, $I_{\rm B3} = 0$ for Λ and Σ^0, and $I_{\rm B3} = -1$ for Σ^-.

According to our phenomenological approach the new couplings should be fixed to reproduce some relevant quantity. We proceed in this way to determine the σ- and ω-Λ couplings. Using hypernuclei data the Λ binding energy can be extrapolated to be $\varepsilon_\Lambda = -28$ MeV at n_0, thus we obtain $g_{s\Lambda} = 2.335$, $g_{w\Lambda} = 2.099$. For the other hyperons there are not accurate experimental data. Different arguments are commonly used to get numerical

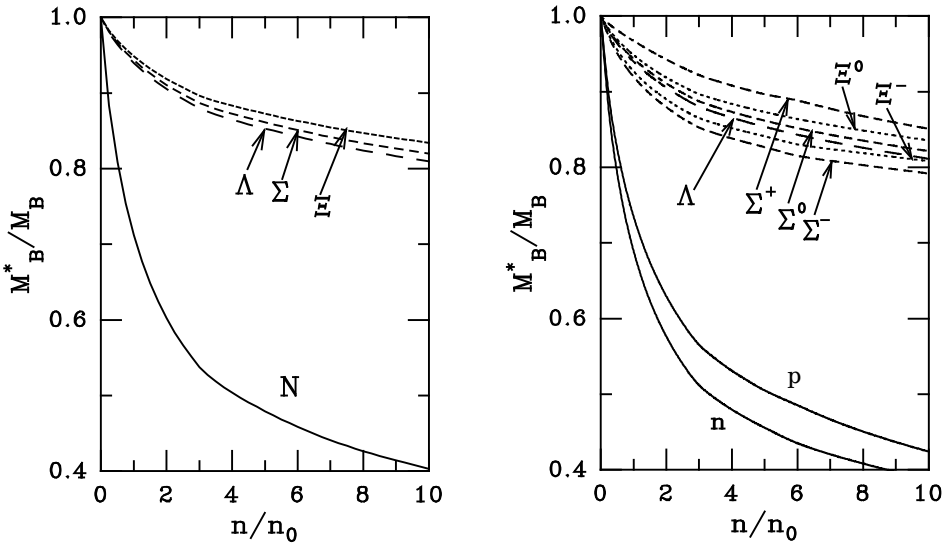

Fig. 9. The effective baryon masses in terms of the total baryon number density. The left (right) panel corresponds to calculations with set A (B). Different type of lines are assigned to each isomultiplet, as indicated in both panels.

values, like $SU(6)$ symmetry or vector meson dominance. For simplicity and to carry out computations, we adopt $g_{s,w\,\Sigma} = g_{s,w\,\Xi} = g_{s,w\,\Lambda}$ and $g_{r,d\,\Sigma} = g_{r,d\,\Xi} = g_{r,d\,\Lambda} = g_{r,d}$, without any further justification. With this choice we obtain very similar binding energies at n_0 : $\varepsilon_\Sigma = -28.11$ MeV, and $\varepsilon_\Xi = -28.27$ MeV for the Σ and Ξ hyperons.

Neutron star matter is electrically neutral and additional contributions coming from electrons and muons must be included. Leptons are treated as Dirac free particles. The equilibrium for β-decay imposes constraints among the baryon and lepton chemical potentials: $\mu_{\rm B} = \mu_n - q_{\rm B}\mu_e$. Here we have used $q_{\rm B}$ for the baryon electric charge in units of the positron charge, μ_n, μ_e, and $\mu_{\rm B}$ represents the chemical potentials for neutron, electron and the baryon B, respectively. On the other hand, the electric charge neutrality imposes $0 = -\sum_{\rm l} n_{\rm l} + \sum_{\rm B} q_{\rm B} n_{\rm B}$, with $n_{\rm l}$ and $n_{\rm B}$ indicating the number density for leptons and baryons. At zero temperature we consider the Fermi momentum $p_{\rm F}$, writing: $n_i = p_{{\rm F}\,i}^3/(3\pi^2)$, $\mu_{\rm l} = \sqrt{p_{\rm Fl}^2 + m_{\rm l}^2}$ for leptons, and $\mu_{\rm B} = \sqrt{p_{\rm F\,B}^2 + M_{\rm B}^{*2}} + g_{w\,{\rm B}}^* \bar{\omega} + g_r^* I_{\rm B3} \bar{\rho}$ for baryons. The efective mass $M_{\rm B}^*$ is a generalization of eq. (10), $M_{\rm B}^* = (M_{\rm B} - I_{\rm B} g_d \bar{\delta})/N_{\rm B}$ with $I_{\rm B} = 1$ for p, Σ^+, and Ξ^0, $I_{\rm B} = 0$ for Λ and Σ^0, and $I_{\rm B} = -1$ for n, Σ^-, and Ξ^-. We have used $N_{\rm B} = 1 + g_{s{\rm B}}\bar{\sigma}/M_{\rm B}$, where $M_{\rm B}$ is the averaged mass of the baryon isomultiplet B.

The effective baryon masses as functions of the baryonic number density are shown in fig. 9. In the results corresponding to set A, each isomultiplet remains degenerate in mass. The variation of the hyperon masses are much more moderate than for the nucleon masses. As a consequence of the specific interaction used, the heavier the baryon considered, the weaker the density dependence of its effective mass is. Using the coupling set B the isospin degeneracy is removed, enhancing or dropping the mass of particles with positive or negative isospin projection, respectively, as it is depicted on the right part of fig. 9.

In fig. 10 the relative population of the baryonic species is shown in terms of the total particle number, at $T = 0$. In the range of densities studied the full baryon octet is present, with exception of the Ξ^0 when the coupling set B is used. The results obtained with $g_d = 0$ and $g_d = 6.538$ are very similar for the leptons and the lightest baryons (p, n, and Λ). Differences between them become noticeable in the growth of populations of the heavier fermions Σ and Ξ. The more obvious is the early appearance, at $n \simeq 3.3\, n_0$, and predominance of Σ^- particles in the results with the coupling set A.

The equilibrium baryonic population is not perturbed by the presence of the δ-meson (set B) at low and medium densities. The effect of turning on the δ interaction, is twofold and is emphasized at high densities. In first place the baryon-δ interaction enhances the effective mass of Ξ^0 and diminishes that of Σ^- and Ξ^-, increasing and lowering the corresponding thresholds. The more evident consequence of this is the absence of Ξ^0 particles in the range $0 < n/n_0 < 10$ (right panel of fig. 10). In second place the coupling g_r grows with g_d, affecting more strongly to the isotriplet $\boldsymbol{\Sigma}$ than the isoduplet $\boldsymbol{\Xi}$, due to the factor $I_{\rm B3}$. Since the ρ-meson contribution to the chemical potential is positive and greater for Σ^- than for Ξ^-, this causes the appearance of Σ^- and of Ξ^- to be delayed and anticipated, respectively, going from the left to the right panel of fig. 10. The Λ and Σ^0 baryons, which do not couple to the isovector mesons, do not show appreciable changes in their distributions. On the other hand, from the comparatively earlier raising of the Σ^+ and Ξ^- population obtained with set B, it is possible to infer that, in absolute values, the δ contribution to the baryonic chemical potentials lies between one-half and the total ρ contribution. Of course, these results are partially a consequence of our assumption of equal couplings g_d and g_r for all the hyperons considered.

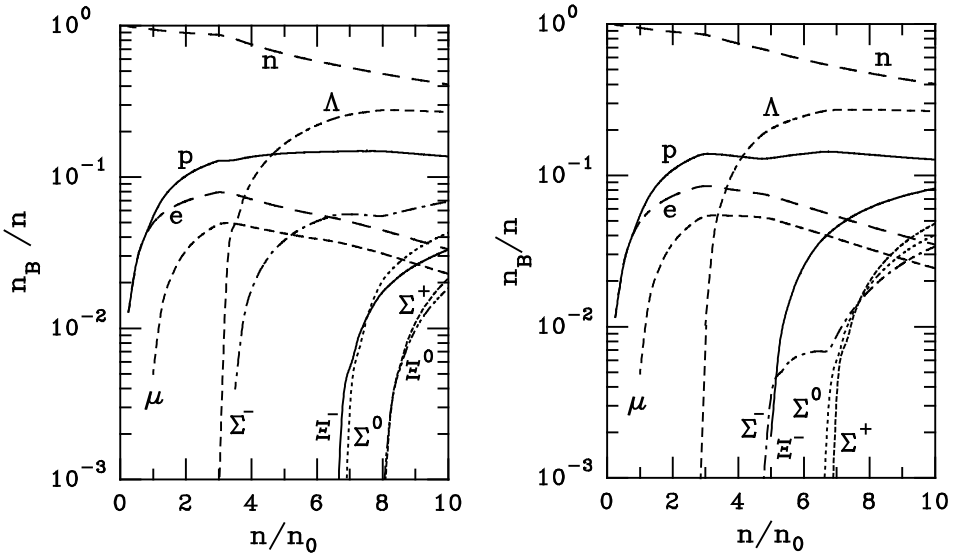

Fig. 10. The fraction of leptons and baryon species present in hadronic matter in β-equilibrium at $T = 0$. The different curves are labeled with the corresponding particle name. The left (right) panel corresponds to calculations with the coupling set A (B).

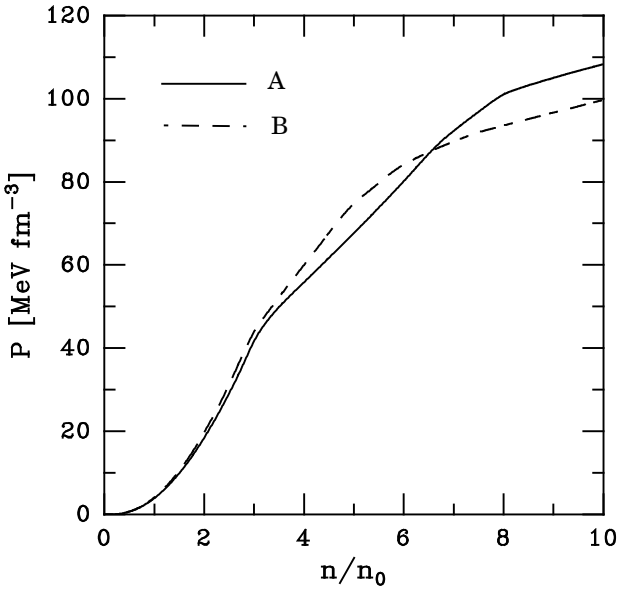

Fig. 11. The pressure of hadronic matter in β-equilibrium at $T = 0$. As indicated in the figure, solid (dashed) line corresponds to calculations using the coupling set A (B).

The pressure in terms of the baryon number density is exhibited in fig. 11. There are abrupt changes of slope in the curve corresponding to the set A, which coincide with the appearance of hyperons. Similar changes, but more attenuated, take place in the curve with the set B.

6 Meson propagation in asymmetric nuclear matter

Medium effects in the meson properties have received attention in the later years, as they could carry the signals of phase transitions in the hadronic environment. As previously stressed, we expect that our results be valid out of the vicinity of the transition point.

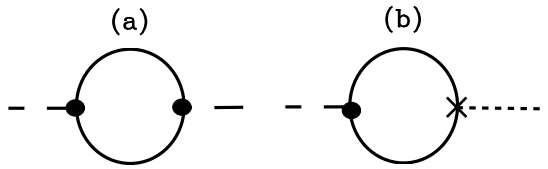

Fig. 12. Feynman diagrams included in the RRPA. Case a (b) corresponds to pure (mixing) meson propagation. The solid line stands for baryon propagator, dashed and dotted lines represent meson propagators of different types, and the filled circle and the cross their respective vertices.

In the MFA mesons are treated as classical fields, with constant mass. In order to include quantum corrections we must go beyond the MFA. This can be done in the relativistic random phase approximation (RRPA), using the linearized residual interaction of eq. (13). In this approach the meson propagators are corrected by incorporating the baryon bubble diagrams at all orders, by using the Dyson-Schwinger equation. From the corrected propagator the effective meson mass can be extracted. This procedure has been applied in QHD calculations, see for example [10] and references listed therein. Specific computations with the DSCM can be found in [14,15].

The one-loop proper polarization insertions comprise the diagrams shown in fig. 12. Case (a) represent the propagation of a pure meson field, and case (b) the mixing amplitude of different mesonic types. Due to baryon current conservation, the proper polarization for all the mesons can be written in terms of a few components. Some of them are divergent and requires an appropriate regularization. For this purpose, we follow the scheme outlined

in [15]. We do not deduce those results here, but we reproduce the main equations for the sake of completeness.

The formalism is best described within a generalized meson propagator, in a matrix representation of dimension equal to the sum of the mesonic degrees of freedom. For example the generalized free meson propagator $\mathcal{P}^0$, has in its diagonal blocks the free meson propagators $S^0(q)$, $D^{0\,\mathrm{AB}}(q)$, $W^0_{\mu\nu}(q)$, and $R^{0\,\mathrm{AB}}_{\mu\nu}(q)$, for the $\sigma(x), \delta(x), \omega(x)$, and $\rho(x)$ fields, respectively, and null matrices in the complementary spaces:

$$\mathcal{P}^0_{\alpha\beta}(q) = \begin{pmatrix} S^0(q) & & & \\ & D^0(q) & & \\ & & W^0(q) & \\ & & & R^0(q) \end{pmatrix}_{\alpha\beta} .$$

A similar expression holds for the full generalized propagator $\mathcal{P}$, but the complementary spaces are filled with the mixing meson propagators:

$$\mathcal{P}_{\alpha\beta}(q) = \begin{pmatrix} S(q) & M_{\sigma\delta}(q) & M_{\sigma\omega}(q) & M_{\sigma\rho}(q) \\ M_{\delta\sigma}(q) & D(q) & M_{\delta\omega}(q) & M_{\delta\rho}(q) \\ M_{\omega\sigma}(q) & M_{\omega\delta}(q) & W(q) & M_{\omega\rho}(q) \\ M_{\rho\sigma}(q) & M_{\rho\delta}(q) & M_{\rho\omega}(q) & R(q) \end{pmatrix}_{\alpha\beta} .$$

The Dyson-Schwinger equation can be used to solve for $\mathcal{P}^{-1}(q)$:

$$\mathcal{P}^{-1}_{\alpha\beta}(q) = \mathcal{P}^{0\,-1}_{\alpha\beta}(q) - \Pi_{\alpha\beta}(q),$$

where we have introduced the generalized polarization insertion

$$\Pi_{\alpha\beta}(q) = \begin{pmatrix} \Pi_s(q) & \Pi_{\sigma\delta}(q) & \Pi_{\sigma\omega}(q) & \Pi_{\sigma\rho}(q) \\ \Pi_{\delta\sigma}(q) & \Pi_d(q) & \Pi_{\delta\omega}(q) & \Pi_{\delta\rho}(q) \\ \Pi_{\omega\sigma}(q) & \Pi_{\omega\delta}(q) & \Pi_w(q) & \Pi_{\omega\rho}(q) \\ \Pi_{\rho\sigma}(q) & \Pi_{\rho\delta}(q) & \Pi_{\rho\omega}(q) & \Pi_r(q) \end{pmatrix}_{\alpha\beta} . \quad (20)$$

Since we are primarily interested in the propagation of the pure meson fields, we neglect mixing polarizations as a first approach. The formulae for the one-loop diagonal components are as follows:

$$i\Pi_s(q) = \sum_{\mathrm{B}} g^{*\,2}_{s\mathrm{B}} \int \frac{\mathrm{d}^4p}{(2\pi)^4} \Big\{ \mathrm{Tr}\left[G_{\mathrm{B}}(q) G_{\mathrm{B}}(q+p)\right] + \sum_{\lambda} \frac{2\bar{\phi}_\lambda}{M_{\mathrm{B}}} \mathrm{Tr}\left[G_{\mathrm{B}}(q) \Gamma_\lambda G_{\mathrm{B}}(q+p)\right] + \sum_{\lambda,\lambda'} \bar{\phi}_\lambda \bar{\phi}_{\lambda'} \mathrm{Tr}\left[G_{\mathrm{B}}(q) \Gamma_\lambda G_{\mathrm{B}}(q+p) \Gamma_{\lambda'}\right] / M^2_{\mathrm{B}} \Big\},$$

$$i\Pi_d^{AC}(q) = g^{*\,2}_d \sum_{\mathrm{B}} \int \frac{\mathrm{d}^4p}{(2\pi)^4} \mathrm{Tr}\left[G_{\mathrm{B}}(q) T^A G_{\mathrm{B}}(q+p) T^C\right],$$

$$i\Pi_w^{\mu\nu}(q) = \sum_{\mathrm{B}} g^{*\,2}_{w\mathrm{B}} \int \frac{\mathrm{d}^4p}{(2\pi)^4} \mathrm{Tr}\left[G_{\mathrm{B}}(q) \gamma^\mu G_{\mathrm{B}}(q+p) \gamma^\nu\right],$$

$$i\Pi_{r\,\mu\nu}^{AC}(q) = g^{*\,2}_r \sum_{\mathrm{B}} \int \frac{\mathrm{d}^4p}{(2\pi)^4} \times \mathrm{Tr}\left[G_{\mathrm{B}}(q) \gamma_\mu T^A G_{\mathrm{B}}(q+p) \gamma^\nu T^C\right],$$

where the index B runs over all the baryons considered, and λ, λ' in the first equation runs over the meson fields δ, ω, and ρ. The vertices Γ_λ have been generalized to hyperons, *i.e.* $\Gamma_\lambda = -g_d I_{\mathrm{B}}, g_{w\mathrm{B}}\gamma, g_r I_{\mathrm{B}3}\gamma$, respectively. The baryon propagators $G_{\mathrm{B}}(q)$ are evaluated in the MFA. In our calculations we only need the transversal component in the Lorentz indices, and the third component of isospin. For this purpose we use $T^3 = \tau^3/2$ for the nucleon and Ξ, $T^3 = 0$ for the Λ, and $T^3 = \mathrm{diag}(1, 0, -1)$ for the Σ-particle. The referred expressions contain particle-antiparticle, particle-hole, and Pauli blocking contributions. The first one is divergent, and to extract finite contributions we apply the regularization scheme outlined in [15]. The Lorentz scalar contributions, containing the integrand $\mathrm{Tr}\left[G_{\mathrm{B}}(q) G_{\mathrm{B}}(q+p)\right]$, remains undefined by a constant λ, related to the covariant derivative of the polarization evaluated at the regularization point. We take this constant as a free parameter to analyze the possible dynamical regimes. There are two independent parameters λ_s and λ_d corresponding to the diagonal components Π_s and Π_d, respectively. We require null contribution for the polarization evaluated on the meson mass shell, at zero baryon density and temperature. Thus we obtain for the finite particle-antiparticle contribution of the baryon-B bubble:

$$\Pi'^{\,00}_{v\mathrm{B}}(q) = \frac{g^{*\,2}_{v\mathrm{B}}}{2\pi^2} q^2 \int_0^1 \mathrm{d}z\, z(1-z)\, \ln\left[\frac{M^{*2}_{\mathrm{B}} - z(1-z)\mathsf{q}^2}{M^2_{\mathrm{B}} - z(1-z) m_v^2}\right],$$

$$\Pi'^{\,33}_{v\mathrm{B}}(q) = \frac{\mathsf{q}^2}{q^2}\, \Pi'^{\,00}_{v\mathrm{B}}(q),$$

$$\Pi'_{c\mathrm{B}}(q) = \lambda_c \frac{g^{*2}_{c\mathrm{B}}}{8\pi^2}(m^{*2}_{\mathrm{B}} m_c^2 - \mathsf{q}^2) - \frac{3 g^{*2}_{c\mathrm{B}}}{4\pi^2} \times \int_0^1 \mathrm{d}z\, [M^{*2}_{\mathrm{B}} - z(1-z)\mathsf{q}^2] \times \ln\left[\frac{M^{*2}_{\mathrm{B}} - z(1-z)\mathsf{q}^2}{M^2_{\mathrm{B}} - z(1-z) m_c^2}\right], \quad (21)$$

where the index $v = w, r$ runs over the vector mesons, and $c = s, d$ runs over the scalar ones. In the case of isovector polarizations, it must be regarded as the (3,3) isospin component. Furthermore we have used $\mathsf{q}^2 = q_\mu q^\mu$, q is the modulus of the spatial component of the momentum, and $m^*_{\mathrm{B}} = M^*_{\mathrm{B}}/M_{\mathrm{B}}$.

Once the polarization has been properly defined, we introduce the effective meson masses m^*_s, m^*_d, m^*_w, and m^*_r. They have been defined as the zeroes of the corresponding inverse propagators at zero vector momentum, *i.e.* the p_0

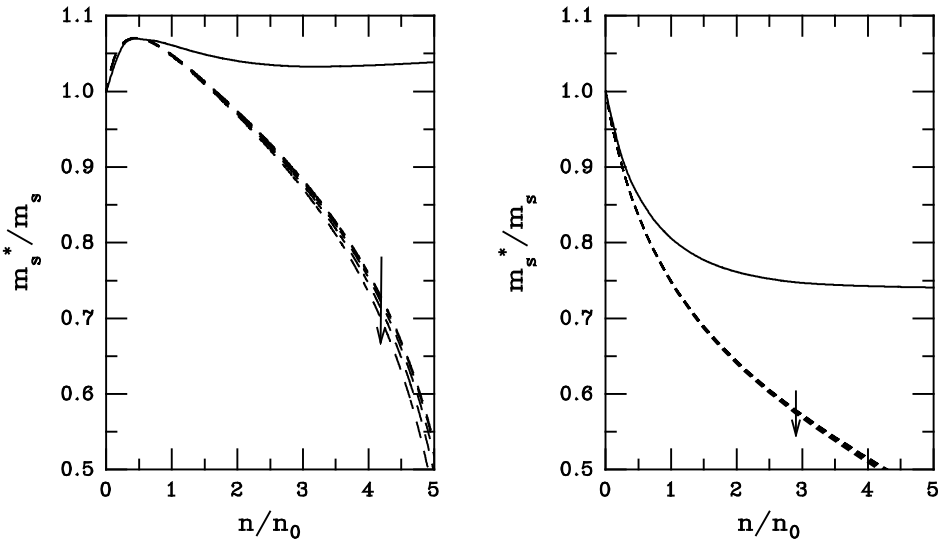

Fig. 13. The effective σ-meson mass as a function of the baryonic density at $T = 0$. In the left (right) panel the results for the regularization parameter $\lambda_s = 10$ ($\lambda_s = 100$) are plotted. In each case the solid line corresponds to hadronic matter in β-equilibrium, and the dashed lines to nuclear matter with asymmetry coefficients $\chi = 0, 0.25, 0.50, 0.75$, and 1. The arrow indicates the direction of growing χ in the last case.

solutions of:

$$\mathcal{P}_{aa}^{-1}(p_0, p = 0) = \mathcal{P}_{aa}^{0\,-1}(p_0, p = 0) - \Pi_{aa}(p_0, p = 0) = 0, \qquad (22)$$

for $a = s, d, w$, and r.

In figs. 13-15 we show the numerical results for the density dependence of the meson masses at $T = 0$, under different compositions of the hadronic medium. In fig. 13 the behavior of the σ-meson mass is presented. The results correspond to the coupling set A, there are no appreciable differences with respect to the calculations using set B.

It can be seen that in β-stable hadronic matter the mass is almost constant at high densities. In the case of nuclear matter at constant asymmetry the density dependence is more pronounced, and monotonously decreasing. The asymmetry dependence is small, as this figure shows.

Figure 14 is devoted to the a_0-meson mass. The curves for matter in β-equilibrium are qualitatively similar to those corresponding to the σ-meson. In asymmetric nuclear matter its behavior is much more striking. For $\lambda_d = 10$ the mass becomes zero at $n/n_0 \simeq 4$, whereas for $\lambda_d = 100$ it decreases sharply but never vanishes in the whole range considered.

The differences shown in figs. 13 and 14, between the choices $\lambda = 10$ and $\lambda = 100$, indicate the ambiguity of the regularization procedure. We have selected these values only as representatives of the qualitatively diverse behaviors that can be obtained for the effective meson masses.

The masses for the vector mesons are shown in fig. 15. For the ω-meson the behavior is almost independent of the composition of the hadronic environment, sensible departures are observed only for extreme densities. This is not the case of the ρ-meson mass, a clear difference among β-stable matter and asymmetric nuclear matter is observed, even at low densities.

Since $\Pi_{aa}(p)$ receives the contribution of all the baryonic species considered, the mesonic effective masses are strongly influenced by the inclusion of hyperons, even at densities close to the normal saturation value. It must be noted that the particle-antiparticle term coming from the baryon-B bubble contributes even when this particle is not present on its Fermi shell. The hyperon particle-antiparticle contributions at medium and high densities produce the stabilization of the mesonic masses in neutral β-stable matter. This can be appreciated in figs. 13-15 where they exhibit a weaker density dependence as compared to nuclear matter results. The magnitude of this effect is distinct for each type of meson, depending on the strength of its coupling to the hyperons.

The relative smallness of the in-vacuum hyperon-meson couplings as compared with the nucleon-meson ones, is the cause of the similitude of the isoscalar meson masses behavior (m_s^*/m_s and m_w^*/m_w) at very low densities, in both the asymmetric nuclear matter (ANM) and the neutral hypermatter (NHM) situations. This is not true for the isovector mesons (m_d^*/m_d and m_r^*/m_r), whose respective couplings g_d, g_r are the same for all the baryons.

There is an increasing departure of the meson mass behavior in the respective ANM and NHM examples, as the density grows. It is due to the faster decrease of the effective nucleon couplings on the one side, together with the greater multiplicity of hyperons on the other. Therefore, the hyperon vacuum contributions become more and more relevant for higher densities. Since nucleon and hyperon vacuum polarizations have opposite signs in the Lorentz scalar channel, m_s^* and m_d^* drop more slowly in NHM, as compared with the ANM case. In the Lorentz vector channel nucleon and hyperon vacuum polarizations add coherently, instead. Thus the decreasing behavior shown for m_w^* and m_r^* in ANM is accentuated in the NHM case.

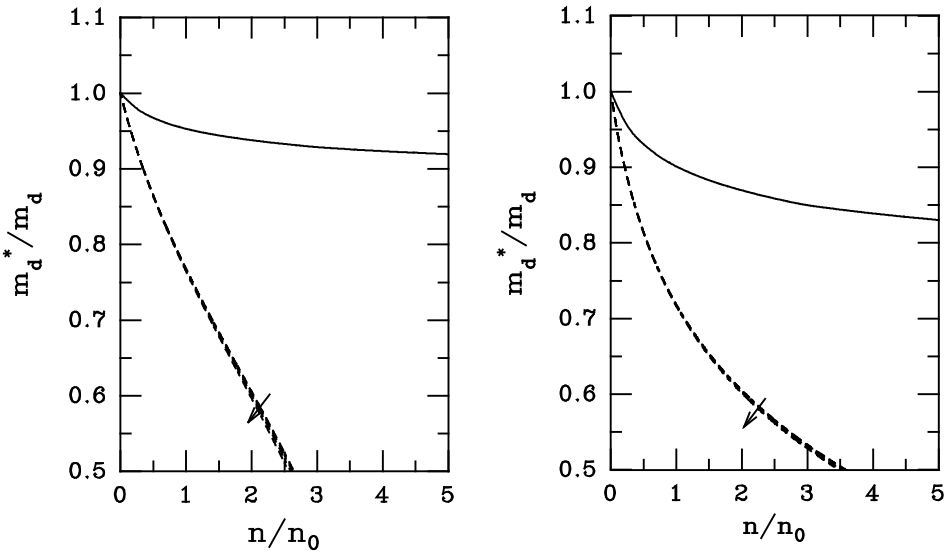

Fig. 14. The effective a_0-meson mass as a function of the density at $T = 0$. The left (right) panel corresponds to the values $\lambda_d = 10$ ($\lambda_d = 100$). Solid line stands for β-stable hadronic matter, and dashed lines correspond to asymmetric nuclear matter with asymmetry $\chi = 0.25, 0.50, 0.75$, and 1. The arrows indicate the direction of growing χ.

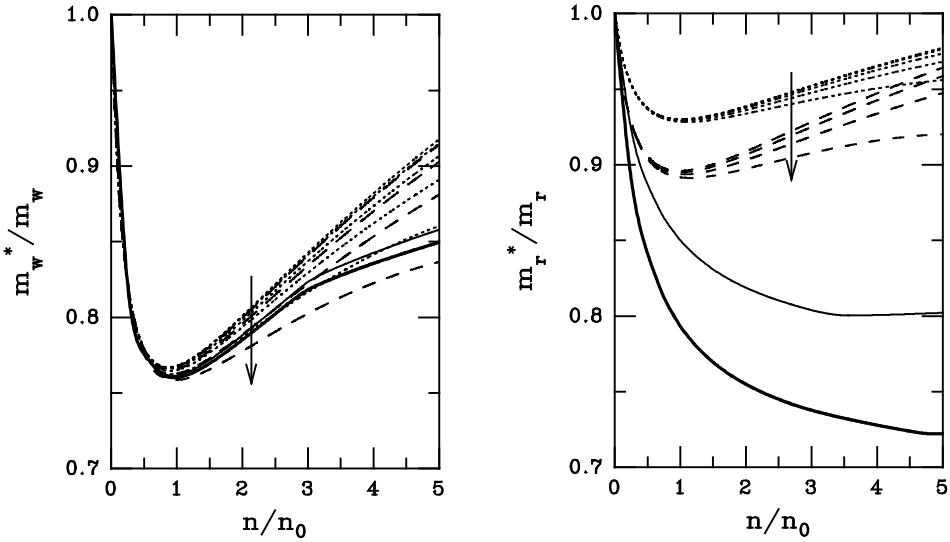

Fig. 15. The density dependence of the vector mesons. The left panel corresponds to the isoscalar ω-meson, the right panel to the isovector ρ-meson. In both cases the bold (thin) solid line corresponds to β-stable matter with coupling set B (A), and dashed (dotted) lines correspond to asymmetric nuclear matter with $\chi = 0, 0.25, 0.50, 0.75$, and 1 using the set B (A). The arrow indicates the direction of growing χ.

Comparison with other theoretical predictions is difficult, since as far as we know meson propagation in isospin asymmetric matter has been poorly studied in the past. We can mention, for instance, the work of ref. [38], where vector meson masses were investigated by including a nucleon-meson tensorial coupling. The Dirac sea contributions to the meson polarizations are also included. As in our results vector meson masses decrease when the asymmetry increases. At $n = 3n_0$ they found a relative change of 6% (17%) in m_w (m_r) when passing from symmetric nuclear matter to pure neutron matter. Instead, we find here a drop of about 2% (6%) for m_w (m_r) at the same conditions. Contrary to our findings, in ref. [38] a fast monotonous decrease of both m_w and m_r is obtained in the range $0 < n/n_0 < 2.5$

Meson properties in symmetric nuclear matter were investigated within the QHD-I model, for example in [39]. This calculation show a monotonous increase of m_s in the range $n \geq n_0$. The disagreement with the qualitative behavior shown in fig. 13 can be assigned mainly to the different schemes of regularization used, and to the strong decrease of the effective coupling g_s^* in the modified DSCM. Instead, the behavior of m_w^* is more alike to ours, since both sources of discrepancy are moderated in the vector channel.

A comparison with the DSCM calculations of [15] shows that the main effect of generalizing the non-linear σ interaction to the vector meson couplings is noteworthy for the effective σ- and ω-meson masses. Their density dependence is more abrupt in the present work, and generally speaking the values obtained here are lower than in ref. [15].

As mentioned before, the results given here are obtained by neglecting the contribution of mixing in the meson polarization. The influence of such effects was previously studied in a variety of works, see for example [38,40, 41]. There, sizeable contributions were found. In order to test our assumptions, we have evaluated the mixing components of eq. (20) at the points $q_0 = m_a^*, q = 0$, where $a = s, w$. We have found that only $\Pi_{\sigma\delta}$ and $\Pi_{\omega\rho}$ give non-zero contributions in such conditions. These contributions remain relatively small for the σ-δ mixing, due to the big difference between their respective masses. On the opposite, our estimates of ω-ρ mixing give significative values in the whole range of densities considered, although it tends to diminish at high densities. This result does not support the assumptions made, and further investigation is needed to determine how much the distribution of zeroes of eq. (22) is modified by the inclusion of mixing terms. Such calculations are out of the scope of the present work, and therefore the results shown in sect. 6 must be taken as a first approach to the full problem.

7 Discussion and summary

In this paper we have proposed an effective relativistic hadronic model inspired in the DSCM to investigate in-medium hadronic properties, in terms of the baryon isospin asymmetry. The non-linear σ-nucleon interaction is generalized to the isoscalar vector, isovector scalar, and isovector vector channels. Effective medium-dependent couplings arise at the MFA, and a residual interaction with one and two-meson exchange is obtained beyond the MFA. The equation of state (EoS) for symmetric nuclear matter is softer than the one corresponding to the DSCM. The symmetry energy coefficient shows an intermediate behavior between the QHD model and non-relativistic variational calculations. The asymmetry dependence of the EoS becomes relevant for densities $n \geq 3n_0$, and it is emphasized by the contribution of the $a_0(980)$-meson exchange. Temperature effects in the range $0 < T < 100$ MeV are noticeable in the EoS, but moderate in the effective baryon masses. As a particular manifestation of asymmetric matter we study hadronic matter with hyperons, in equilibrium against electroweak decay at $T = 0$. The δ coupling is the cause of notable modifications in the population of hyperons at high densities. Due to the lower hyperon-meson couplings, relative to the nucleon-meson ones, the hyperonic effective masses decrease more moderately as the baryon density increases.

The effective meson masses have been evaluated at $T = 0$ in the RRPA, including particle-antiparticle finite contributions. The regularization procedure left undefined parameters λ_s and λ_d. We have selected numerical values for them, which differ by one order of magnitude, and are representative of the possible dynamical regimes. In asymmetric nuclear matter the scalar σ- and δ-mesons exhibit monotonous decreasing masses for high densities, whereas the vector ω- and ρ-meson masses show a slight increase for $n/n_0 > 1$. In all cases the effective masses remain below its vacuum values at extreme densities. The dependence on the asymmetry χ is more evident for the vector mesons. In β-stable hadronic matter the density variation of the effective masses of all the mesons considered is damped, becoming approximately constants at twice the saturation density. This effect is due to the particle-antiparticle terms, contributing even for particles out of their Fermi shell.

Since our calculations do not include mixing effects, additional investigation is required to properly include σ-δ and ω-ρ polarization in the determination of the effective meson masses in the modified DSCM.

This work was partially supported by the CONICET, Argentina.

References

1. R. Brockmann, H. Toki, Phys. Rev. Lett. **68**, 3408 (1992); G.Q. Li, R. Machleidt, Y.Z. Zhuo, Phys. Rev. C **48**, 1062 (1993).
2. S. Haddad, M.K. Weigel, Phys. Rev. C **48**, 2740 (1993).
3. H. Lenske, C. Fuchs, Phys. Lett. B **345**, 355 (1995); C. Fuchs, H. Lenske, H.H. Wolter, Phys. Rev. C **52**, 3043 (1995); F. de Jong, H. Lenske, Phys. Rev. C **58**, 890 (1998), and references therein.
4. F. de Jong, H. Lenske, Phys. Rev. C **57**, 3099 (1998).
5. F. Hoffmann, C.M. Keil, H. Lenske, Phys. Rev. C **64**, 034314 (2001).
6. S. Typel, S.S. Wolter, Nucl. Phys. A **656**, 331 (1999).
7. M.K. Banerjee, Phys. Rev. C **45**, 1359 (1992); M.K. Banerjee, J.A. Tjon, Phys. Rev. C **56**, 497 (1997).
8. A.M. Rakhimov, F.C. Khanna, U.T. Yakhshiev, M.M. Musakhanov, Nucl. Phys. A **643**, 383 (1998).
9. K. Saito, A.W. Thomas, Phys. Lett. B **327**, 9 (1994).
10. B.D. Serot, J.D. Walecka, Int. J. Mod. Phys. E **6**, 515 (1997).
11. G.E. Brown, M. Rho, Phys. Rev. Lett. **66**, 2720 (1991).
12. H. Feldmeier, J. Lindner, Z. Phys. A **341**, 83 (1991).
13. J. Zimanyi, S.A. Moszkowski, Phys. Rev. C **42**, 1416 (1990).
14. A. Bhattacharyya, S. Raha, Phys. Rev. C **53**, 522 (1996).
15. R. Aguirre, Phys. Rev. C **63**, 025206 (2001).
16. R. Aguirre, A.L. De Paoli, O. Civitarese, Nucl. Phys. A **597**, 543 (1996).
17. G.E. Brown, M. Rho, Nucl. Phys. A **596**, 503 (1996); G.E. Brown, M. Buballa, M. Rho, Nucl. Phys. A **609**, 519 (1996).
18. R. Rapp, J.W. Durso, J. Wambach, Nucl. Phys. A **615**, 501 (1997); H.C. Chiang, E. Oset, M.J. Vicente Vacas, Nucl. Phys. A **644**, 77 (1998); P. Schuck, Z. Aouissat, F. Bonutti, G. Chanfray, E. Fragiacomo, N. Grion, J. Wambach, LANL report nucl-th/9806069; M.J. Vicente Vacas, E. Oset, Phys. Rev. C **60**, 064621 (1999); R. Rapp,

R. Machleidt, J.W. Durso, G.E. Brown, Phys. Rev. Lett. **82**, 1827 (1999); M.J. Vicente Vacas, E. Oset, LANL report nucl-th/0002010; D. Davesne, Y.J. Zhang, G. Chanfray, Phys. Rev. C **62**, 024604 (2000); P. Schuck, Z. Aouissat, G. Chanfray, J. Wambach, LANL report nucl-th/0002031; Z. Aouissat, G. Chanfray, P. Schuck, J. Wambach, Phys. Rev. C **61**, 012202 (2000).
19. G. Gelmini, B. Ritzi, Phys. Lett. B **357**, 431 (1995).
20. J.M. Lattimer, C.J. Pethick, M. Prakash, P. Haensel, Phys. Rev. Lett. **66**, 2701 (1991).
21. M. Prakash, T.L. Ainsworth, J.M. Lattimer, Phys. Rev. Lett. **61**, 2518 (1988).
22. J.-K. Zhang, D.S. Onley, Phys. Rev. C **44**, 2230 (1991); M.M. Sharma, S.A. Moszkowski, P. Ring, Phys. Rev. C **44**, 2493 (1991); K. Miyazaki, Prog. Theor. Phys. **91**, 1271 (1994); **93**, 137 (1995); R.J. Lombard, S. Marcos, J. Mares, Phys. Rev. C **51**, 1784 (1995); P. Bernardos, R.J. Lombard, M. Lopez-Quelle, S. Marcos, R. Niembro, Phys. Rev. C **62**, 024314 (2000).
23. N.K. Glendenning, F. Weber, S.A. Moszkowski, Phys. Rev. C **45**, 844 (1992); M. Prakash, J.R. Cooke, J.M. Lattimer, Phys. Rev. D **52**, 661 (1995).
24. S.K. Choudhury, R. Rakshit, Phys. Rev. C **48**, 598 (1993).
25. M. Barranco, R.J. Lombard, S. Marcos, S.A. Moszkowski, Phys. Rev. C **44**, 178 (1991).
26. R. Aguirre, M. Schvellinger, Phys. Lett. B **400**, 245 (1999).
27. T.S. Biro, J. Zimanyi, Phys. Lett. B **391**, 1 (1997).
28. B.D. Serot, J.D. Walecka, Nucl. Phys. A **663**, 513 (2000); R.J. Furnstahl, B.D. Serot, Nucl. Phys. A **671**, 447 (2000).
29. S. Kubis, M. Kutschera, Phys. Lett. B **399**, 191 (1997).
30. M. Kutschera, J. Niemiec, Phys. Rev. C **62**, 025802 (2000).
31. B.-A. Li, C.M. Ko, Z. Ren, Phys. Rev. Lett. **78**, 1644 (1997).
32. B.-A. Li, C.M. Ko, W. Bauer, Int. J. Mod. Phys. E **7**, 147 (1998); B.-A. Li, Phys. Rev. Lett. **85**, 4221 (2000).
33. M. Kutschera, W. Wojcik, Phys. Lett. B **223**, 11 (1989).
34. M. Kutschera, Phys. Lett. B **340**, 1 (1994).
35. C.-H. Lee, T.T.S. Kuo, G.Q. Li, G.E. Brown, Phys. Rev. C **57**, 3488 (1998).
36. V. Greco, M. Colonna, M. Di Toro, G. Fabbri, F. Matera, Phys. Rev. C **64**, 045203 (2000).
37. R.B. Wiringa, V. Fiks, A. Fabrocini, Phys. Rev. C **38**, 1010 (1988).
38. A.K. Dutt-Mazumder, Nucl. Phys. A **611**, 442 (1996).
39. K. Saito, T. Maruyama, K. Soutome, Phys. Rev. C **40**, 407 (1989).
40. A.K. Dutt-Mazumder, B. Dutta-Roy, Phys. Lett. B **399**, 196 (1997); Phys. Rev. C **63**, 015204 (2001); O. Teodorescu, A.K. Dutt-Mazumder, C. Gale, Phys. Rev. C **61**, 051901 (2000); **63**, 034903 (2001); A.K. Dutt-Mazumder, C. Gale, O. Teodorescu, LANL report nucl-th/0008056.
41. W. Broniowski, W. Florkowski, Phys. Lett. B **440**, 7 (1998)